Terahertz Dual-Band Metamaterial Biosensor for Cervical-Cancer Diagnostics

Musa N. Hamza ⓘ, Mohammad Alibakhshikenari ⓘ, *Member, IEEE*, Bal Virdee ⓘ, Muhamad A. Hamad ⓘ, Salahuddin Khan ⓘ, Slawomir Koziel ⓘ, and Ernesto Limiti ⓘ, *Senior Member, IEEE*

Abstract—This study highlights the potential of employing terahertz metamaterial structures as dual-band biosensors for the early detection of cancerous biological tissue. The fundamental principle leveraged here is the alteration of the effective dielectric constant of biological tissue by cancerous cells. The change in the dielectric constant, in turn, induces a shift in the resonance frequency of the metamaterial sensor. One notable advantage of the terahertz metamaterial sensor is its relatively compact size compared to other sensor types, as its dimensions are independent of the wavelength. This property translates into a requirement for a much smaller biopsy sample, facilitating less invasive testing procedures. Beyond the size advantage, the proposed biosensor demonstrates efficacy in detecting abnormalities within biological tissue.

Index Terms—Biosensors, terahertz, metamaterials, cancer.

I. INTRODUCTION

THE World Health Organization (WHO) estimates that approximately 10 million people worldwide died from cancer in 2020. Cancer is a complex disease that affects various bodily systems, characterized by the uncontrolled growth of abnormal cells. These malignant cells have the potential to cause organ failure and death. However, early identification and

Musa N. Hamza is with the Department of Physics, College of Science, University of Raparin, Sulaymaniyah 46012, Iraq (e-mail: musa.nuraden @uor.edu.krd).

Mohammad Alibakhshikenari and Ernesto Limiti are with the Electronics Engineering Department, University of Rome "Tor Vergata", 00133 Rome, Italy (e-mail: alibakhshikenari@ing.uniroma2.it; limiti@ing.uniroma2.it).

Bal Virdee is with the Department of Center for Communications Technology, London Metropolitan University, N7 8DB London, U.K. (e-mail: b.virdee@londonmet.ac.uk).

Muhamad A. Hamad is with Physics Department, College of Education, Salahaddin University, Erbil 44002, Iraq (e-mail: muhamad.hamad@su.edu.krd).

Salahuddin Khan is with the College of Engineering, King Saud University, Riyadh 11421, Saudi Arabia (e-mail: drskhan@ksu.edu.sa).

Slawomir Koziel is with the Engineering Optimization & Modeling Center, Reykjavik University, 102 Reykjavik, Iceland, and also with the Faculty of Electronics, Telecommunications and Informatics, Gdansk University of Technology, 80-233 Gdansk, Poland (e-mail: koziel@ru.is).

Digital Object Identifier 10.1109/JPHOT.2024.3458455

prompt treatment of these malignant cells could significantly improve survival rates, especially for breast cancer patients [1]. Currently, traditional methods such as physical examinations, hematology analyses, ultrasound imaging, histopathology, and cytology are the primary means of early cancer detection. While these methods can enhance patient survival and cure rates, they often come with adverse side effects. Imaging techniques such as computed tomography (CT) scans emit substantial radiation, increasing the risk of cancer. Magnetic resonance imaging (MRI) and positron emission tomography (PET) scans, although effective, are often not accessible due to high associated costs [2]. Additionally, blood tests for tumor detection may be less effective in certain types of cancer due to the lack of relevant blood-based biomarkers. Consequently, researchers are focusing on developing biosensors for early disease detection [2].

Cervical cancer is the fourth most common cancer in women worldwide and the leading cause of female cancer-related deaths. Recognizing the importance of early detection and precise diagnosis in improving patient outcomes and reducing mortality rates, addressing this challenge is of paramount importance. Cervical cancer is highly prevalent, especially in resource-limited regions, where limited access to healthcare facilities and diagnostic tools exacerbates the problem. The disease is strongly associated with modifiable risk factors, particularly persistent human papillomavirus (HPV) infection.

Despite significant advances in cervical cancer prevention and control, such as HPV vaccination, cervical cancer remains a prevalent and potentially lethal disease. Therefore, the development of improved diagnostic tools, especially those adaptable and feasible in diverse healthcare settings, is crucial [1], [3].

In the field of biosensing and diagnostics, the terahertz (THz) region, spanning from 0.1 to 10 THz, remains relatively unexplored. THz waves possess unique properties that make them ideal for biomedical applications, including low tissue absorption, a low ionization threshold, and the ability to interact with molecular structures. These properties open up opportunities for creating highly sensitive and precisely targeted biosensors with the potential to revolutionize disease diagnosis, including cervical cancer [4].

Metamaterials, artificially synthesized structures with exceptional optical properties surpassing those of natural materials, are critical in this context [5]. By engineering their unit structures, it is possible to modulate the electromagnetic response of incident waves and enhance interaction with the substance being measured on the metamaterial's surface. This interaction is most

pronounced when the metamaterial's resonant frequency aligns with the characteristic frequency of the substance being measured. Terahertz metamaterial sensors are becoming a significant focus of research, benefiting from advancements in micro/nano fabrication [6].

Metamaterial-based sensors have garnered significant attention in recent years due to their unique ability to manipulate electromagnetic waves in ways not possible with natural materials. These artificially engineered structures possess sub-wavelength features that enable them to exhibit extraordinary electromagnetic properties, such as negative refractive index and enhanced light-matter interactions. One of the key advantages of metamaterial-based sensors is their ability to achieve high sensitivity and specificity in detecting minute changes in the surrounding environment, making them highly suitable for applications in biomedical diagnostics, environmental monitoring, and chemical detection. For instance, Liu et al. in [7] demonstrated a terahertz metamaterial biosensor capable of detecting protein molecules at picomolar concentrations by exploiting the strong localized electromagnetic fields generated by the metamaterial structure. Similarly, Landy et al. in [8] showcased a metamaterial-based perfect absorber that operates at microwave frequencies, which can be tuned to detect small changes in dielectric properties, highlighting the versatility of these sensors. The ability of metamaterials to support high-Q resonances, as explored by Al-Naib et al. in [9], further enhances their application in sensing, allowing for the precise detection of subtle variations in the refractive index of the surrounding medium. These features make metamaterial-based sensors a powerful tool in advancing sensing technologies across various fields.

Consequently metamaterial-based biosensors have also emerged as promising platforms for early disease detection due to their ability to manipulate electromagnetic waves at subwavelength scales. Recent studies have demonstrated the potential of incorporating quasi-bound states in the continuum (QBIC) into metasurface designs to enhance light-matter interactions and improve biosensing performance [10]. By leveraging QBIC resonances, these sensors can achieve increased sensitivity and specificity in detecting biomarkers associated with diseases such as cancer. However, addressing the complexities of biological samples remains a significant challenge in terahertz biosensing. The three-step one-way model proposed by [11] offers a systematic approach to overcoming issues related to sample heterogeneity and interference. By integrating this model with metamaterial-based biosensors, it is possible to develop robust and reliable diagnostic tools for early disease detection.

The concept of achieving high Q-factor resonances through metamaterial design, as demonstrated in [12], is crucial for enhancing the sensitivity and specificity of biosensors. High Q-factors allow metamaterial-based sensors to detect subtle changes in the surrounding medium more effectively. While the primary focus of [12] is on refractive index sensing, the underlying principles of metamaterial design for achieving high Q-factor resonances can be adapted for biosensing applications.

In cancer diagnosis, where different types and stages are characterized by unique biomarkers and molecular profiles, traditional single-frequency biosensors often struggle to capture
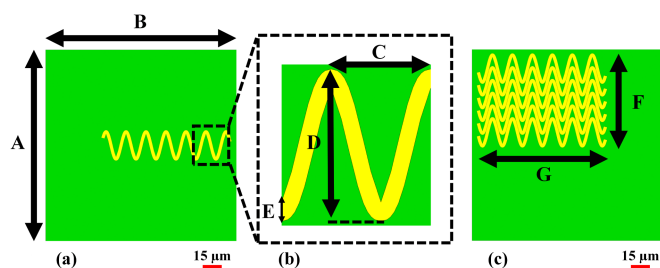

Fig. 1. Proposed metamaterial model#1 of a perfect absorber showing a single wave; (a) one wave, (b) one λ, and (c) model#2.
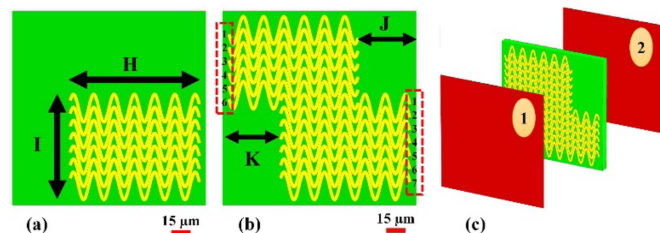

Fig. 2. A perfect metamaterial absorber; (a) model#1, (b) the proposed biosensor model#3, and (c) the proposed model#3 biosensor with input and output ports.

this complexity. To enhance sensitivity and accuracy, we have developed a dual-band biosensor based on metamaterial (MTM) technology. This biosensor shows great promise in addressing the heterogeneity of cancer types and stages by detecting these unique biomarkers. The numerical model used in this study is based on the well-established Finite Difference Time Domain (FDTD) technique, implemented through CST Microwave Studio Suite—an electromagnetic simulation tool widely recognized for its precision and accuracy, consistently validated by strong correlations with experimental results.

In summary, this study demonstrates the feasibility and advantages of using terahertz (THz) metamaterial structures as biosensors. These structures can detect early signs of cancer through resonance frequency modulation, highlighting their potential to improve diagnostic procedures with reduced invasiveness.

II. METAMATERIAL UNIT CELL

The construction of biosensors is complicated and limited by the need for high sensitivity and specificity. Therefore, it is important to enhance the performance of biosensors to improve clinical performance and provide useful information for cervical cancer diagnosis. The proposed biosensor design will consider enhancing the accuracy which is necessary to provide reliable diagnosis of cervical cancer.

Fig. 1(a) and (b) illustrate a conceptual model, referred to as model#1, representing a metamaterial absorber designed for sensing applications. Fig. 1(c) introduces model#2. The integration of model#1 with model#2 results in the formation of a perfect metamaterial absorber, model#3, as depicted in Fig. 2(b). This strategic combination creates two distinct bands within the terahertz frequency range. The composite absorber consists of

TABLE I
OPTIMIZED PHYSICAL PARAMETERS OF THE METAMATERIAL SENSOR

Parameter	Value (μm)	Parameter	Value (μm)
A	150	I	84
B	150	J	44
C	15.6	K	44
D	23.5	Sensor thickness (T1) (see Fig.17)	10
E	2.6	Coverslip thickness (T2) (see Fig.17)	1
F	74	HeLa Cells thickness (T3) (see Fig.17)	7
G	103	Aluminum (Al) thickness	0.2
H	103		

Fig. 3. Absorption spectra of the two designs: (a) model#1, and (b) model#2.

a dielectric metamaterial layer sandwiched between conductive layers. The key parameters defining the characteristics of these models are detailed in Table I. The structure was optimized using a comprehensive full-wave 3D electromagnetic solver, CST Microwave Studio Suite by Dassault Systèmes.

Quantitative calculations are employed to analyze the properties of metamaterials and elucidate their behavior across varying frequency and size ranges. The literature extensively documents the investigation of different configurations, including unit cells, empty spaces, periodic arrays, and perfect electric and magnetic conductors (PEC and PMC) [7], [8], [9].

To streamline simulation processes, a unit cell was defined in the x- and y-directions, while an open space was incorporated in the z-direction. The three-layered model comprises a dielectric spacer at its core, composed of polyethylene terephthalate (PET), flanked by two Aluminum (Al) layers of 0.2 μm thickness. PET is characterized by a low electrical conductivity of approximately 1×10^{12} S/m, reflecting its insulating properties. The thickness of the dielectric spacer used is 10 μm. To optimize performance, one of the Al layers needs to be engineered to exhibit an impedance compatible with the incident medium, facilitating maximum power penetration into and dispersion throughout the PET. Concurrently, the other Al layer serves as a barrier, designed to block all incident electromagnetic (EM) waves and eliminate transmission line interference (TLT). Electromagnetic waves transmitted through the model are terminated at a port featuring high electrical and/or magnetic loss. Through subjecting the model to electromagnetic waves, the absorption parameters of the model can be systematically determined and evaluated.

PET was selected for its optimal combination of dielectric, mechanical, and thermal properties, as well as its biocompatibility and cost-effectiveness. These attributes ensure minimal signal loss, maintain structural integrity, and enable safe interaction with biological tissues, thereby facilitating the sensor's reliable and efficient operation in various conditions.

In this study, the FDTD technique was employed for numerical modeling using CST Microwave Studio Suite. Accurate material properties were utilized to characterize the metamaterial unit cell at terahertz frequencies. Aluminum (Al) was chosen
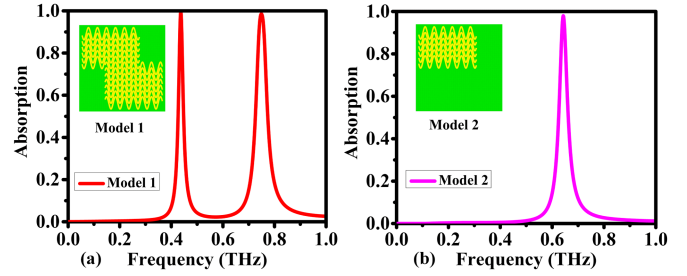
as the conductive material, with an electrical conductivity of 3.77×10^7 S/m. The frequency-dependent permittivity of Aluminum was modeled using the Drude model, which describes the material's response to electromagnetic waves and is defined by the following equation [13]:

$$\epsilon(\omega) = \epsilon_\infty - \frac{\omega_p^2}{\omega^2 + i\gamma\omega} \quad (1)$$

Where $\epsilon(\infty)$ is the high-frequency permittivity, ω_p is the plasma frequency, γ is the collision frequency, and ω is the angular frequency.

Key parameters included a plasma frequency of 2.24×10^{15} rad/s and a collision frequency of 1.22×10^{14} rad/s, which are essential for accurately capturing the behavior of metals at terahertz frequencies.

The feasibility of the proposed biosensor relies on the integration of advanced materials, fabrication techniques, and computational modeling. By leveraging established metamaterial principles, the design achieves a compact form factor suitable for integration into existing diagnostic platforms. As will be shown later, the careful selection of materials and optimization through simulation have resulted in a device with high sensitivity and specificity, highlighting its potential for clinical application.

III. RESULTS AND DISCUSSION

The expression used for modeling wave absorption in the biosensor within CST Microwave Studio Suite was:

$$A = 1 - R - T = 1 - |S_{11}|^2 - |S_{21}|^2 \quad (2)$$

The S-parameters for reflection and transmission are denoted by S_{11} and S_{21}, respectively. The reflection coefficient should be kept as low as possible to achieve maximal absorption.

To investigate the impact of resonator design on absorption capacity within the terahertz (THz) region, we examined twelve distinct models, as shown in Figs. 3 through 7. This exploration is essential for understanding the behavior and efficiency of THz metamaterials as perfect absorbers, requiring thorough characterization and performance assessment. The detailed analysis of these models provides valuable insights into the factors influencing signal resonance at various THz frequencies. This knowledge is crucial for refining design and manufacturing processes to achieve the desired absorption characteristics within this frequency range.
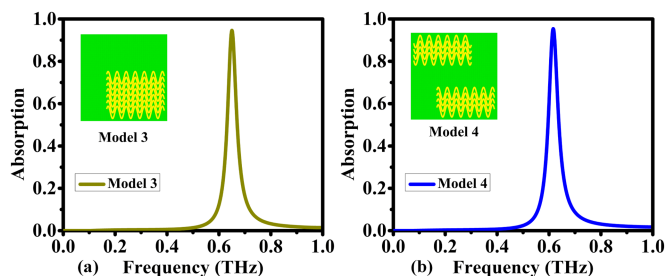
Fig. 4. Absorption spectra of the two designs: (a) model#3, and (b) model#4.
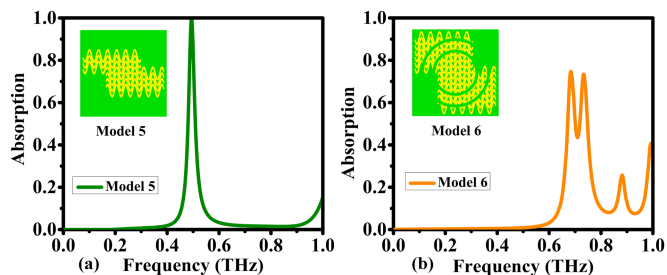

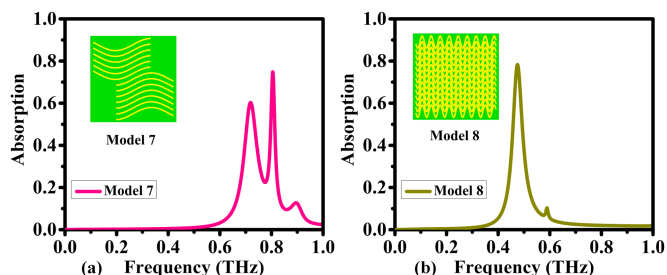Fig. 5. Absorption spectra of the two designs: (a) model#5, and (b) model#6.

Fig. 6. Absorption spectra of the two designs: (a) model#7, and (b) model#8.
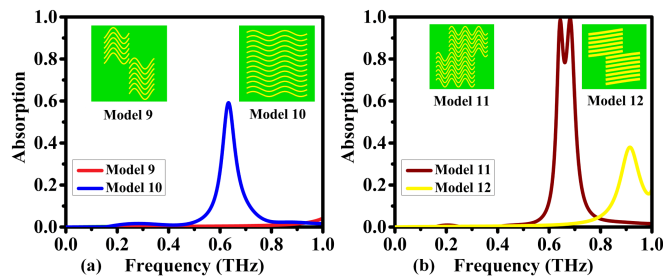

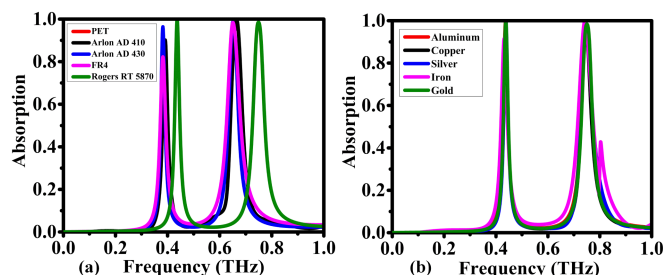Fig. 7. Absorption spectra of the two designs: (a) models#9 & #10, and (b) models#11 & #12.

Fig. 8. Absorption spectra of the models: (a) using different substrate materials, and (b) using different metals as resonators.

The first model, depicted in Fig. 3(a), exhibits two peaks at approximately 0.437 THz and 0.75 THz, with absorption rates exceeding 99.7% and 98.4%, respectively. In contrast, the second model, shown in Fig. 3(b), displays a single peak around 0.65 THz, achieving over 98% absorption. The third model, illustrated in Fig. 4(a), features a solitary peak at approximately 0.65 THz with an absorption rate above 90%. Similarly, the fourth model, shown in Fig. 4(b), has a single peak at about 0.63 THz, also surpassing 90% absorption.

The fifth model, depicted in Fig. 5(a), presents a single peak near 0.5 THz, achieving more than 99% absorption. The sixth model, shown in Fig. 5(b), incorporates two split-ring resonators, resulting in four peaks at around 0.65 THz, 0.75 THz, 0.9 THz, and 1 THz. However, this model does not reach perfect absorption, with an overall capacity below 80%.

The seventh model, shown in Fig. 6(a), reveals two peaks at approximately 0.7 THz and 0.8 THz, while the eighth model in Fig. 6(b) shows a single peak at around 0.5 THz. Both models, despite their peak counts, fail to meet the criteria for perfect absorption, with absorption capacities remaining below 80%.

The ninth and tenth models, depicted in Fig. 7, each exhibit a singular peak around 0.65 THz but do not achieve the threshold for perfect absorption at 80%. The eleventh model, shown in Fig. 7(a), resonates at around 0.63 THz and 0.72 THz, with absorption rates surpassing 98% and 99%, respectively. However, the proximity of these peaks introduces low resolution in microwave imaging, making it unsuitable for distinguishing healthy cells from malignant ones. Finally, the twelfth model, shown in Fig. 7(b), resonates at approximately 0.92 THz but falls short of perfect absorption, with a capacity below 80%.

Fig. 8 demonstrates the impact of substrate and resonator materials on the biosensor's absorption spectrum. The choice of substrate significantly influences resonant behaviour by altering the effective permittivity, which is a measure of how the material polarizes in response to an electric field. This change in effective permittivity modifies the resonance frequency by affecting the propagation speed and wavelength of electromagnetic waves within the sensor, which in turn impacts the peak absorption and bandwidth. A higher effective permittivity typically lowers the resonance frequency, leading to a shift in the absorption spectrum. The conductivity and plasmonic properties of the resonator material play a crucial role in determining the sharpness of the peaks and the intensity of the local electromagnetic fields. Materials with high conductivity and strong plasmonic activity, such as noble metals, support pronounced surface plasmon resonances, resulting in sharper and more intense absorption peaks. These factors collectively influence the biosensor's sensitivity, as the ability to detect subtle changes in the biological environment relies on these sharp, well-defined resonance peaks. By carefully selecting the substrate and resonator materials, the
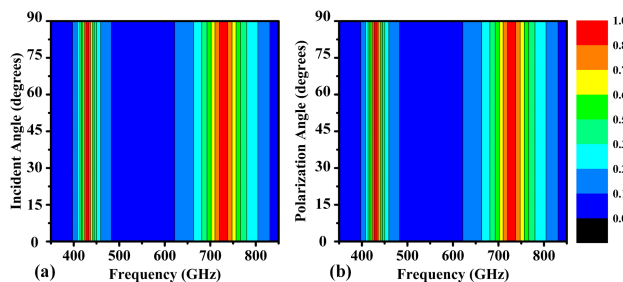
Fig. 9. The impact of angle modification on absorption rate at: (a) incidence angle, and (b) polarization angle.
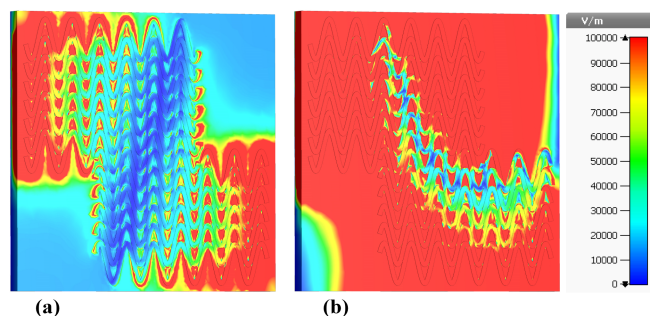

Fig. 10. Distributions of the electric field across the proposed metamaterial structure: (a) E-field at 0.437 THz, and (b) E-field at 0.75 THz.
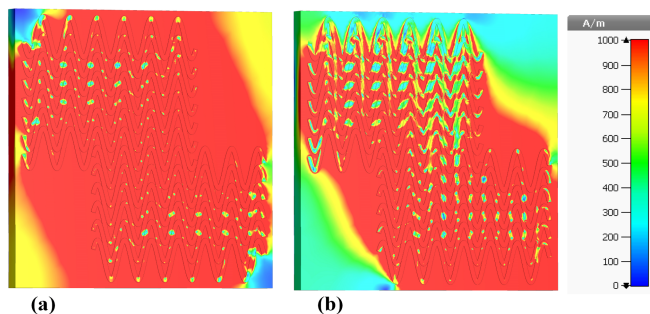

Fig. 11. An illustrated color map showing the magnetic field distribution over the proposed metamaterial structure: (a) H-field at 0.437 THz, and (b) H-field at 0.75 THz.

biosensor's performance can be optimized for high sensitivity and specificity, crucial for effective cancer diagnosis.

Several dielectric substrates were evaluated as potential candidates for the metamaterial absorber, including PET, Arlon AD 410, Arlon AD 430, FR-4, and Rogers RT5780. The absorption spectra for these materials are shown in Fig. 8(a). As expected, FR-4 performed comparatively poorly, as it is more suitable for low-frequency applications.

The study also investigated the impact of different metals on the resonators, considering Aluminium, Copper, Silver, Iron, and Gold. The results, depicted in Fig. 8(b), show minimal variation in absorption characteristics among the metals, except for Iron, which introduced a small third resonance near the second peak. Overall, the choice of metal has a limited impact on the resonator's absorption characteristics, with Iron being the notable exception.

The absorption rate was evaluated across different incident and polarization angles, revealing how changes in angle affect the resonance conditions. Fig. 9 illustrates the biosensor's angular sensitivity and polarization dependence, which are influenced by the underlying physics of permittivity, resonance, and plasmonics. The effective permittivity of the substrate and the plasmonic properties of the resonator material play a crucial role in this behavior. Variations in incident angle alter the phase matching conditions, which can shift the resonance frequency and affect the intensity of absorption peaks. Similarly, the polarization of light impacts the coupling efficiency with surface plasmon resonances, with certain polarizations enhancing or diminishing the local electromagnetic fields. Consistent performance across these varying angles, as demonstrated in the results, indicates that the biosensor maintains stable resonance behavior and strong plasmonic responses under diverse experimental conditions. This robustness is essential for practical applications, ensuring reliable detection sensitivity and accuracy regardless of the specific orientation or polarization of incident light, which is critical for real-world scenarios such as cancer diagnosis.

Polarization can significantly affect the signal-to-noise ratio (SNR) in sensing and imaging applications, potentially leading to distorted results. The symmetrical construction recommended in references [14] and [15] aligns the sensor with polarization effects. Notably, the absorption properties remain consistent

even as the polarization angle varies between 0° and 90° as shown in Fig. 9.

Fig. 9(a) shows that key absorption areas remain stable regardless of orientation, and Fig. 9(b) confirms this consistency across different angles. This stability suggests the model's effectiveness across a wide range of incidence angles and polarizations, efficiently absorbing and transferring incident energy regardless of the wave's orientation or direction.

Figs. 10 and 11 demonstrate the proposed sensor's exceptional performance, particularly in biomedical applications, due to its high electric field density. These field distributions provide valuable insights into the resonance process and deepen our understanding of THz electromagnetic absorbers. By analysing the electric and magnetic field strengths at specific frequencies, we can better understand how the metamaterial structure contributes to signal resonances, which is essential for optimizing biosensor design.

Fig. 10 shows the electric field (E-field) distributions at resonant frequencies of 0.437 THz and 0.75 THz, revealing regions of high field intensity that are essential for efficient energy transfer to the biological medium. These high-intensity regions are a direct result of the resonator's plasmonic properties and the local enhancement of the electromagnetic field, which are critical for maximizing the interaction with target biomolecules. Identifying these regions allows for the optimization of the biosensor's design, enhancing its sensitivity by ensuring that the strongest fields are concentrated where the biological interactions occur.
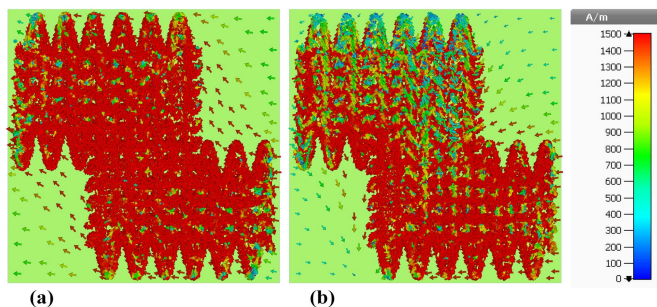
Fig. 12.   The surface current distribution over the proposed metamaterial structure: (a) at 0.437 THz, and (b) at 0.75 THz.

Fig. 13.   Power flow over the proposed metamaterial structure: (a) at 0.437 THz, and (b) at 0.75 THz.

Fig. 11 shows the magnetic field (H-field) distributions at the same resonant frequencies, providing insights into the magnetic response of the metamaterial structure. The H-field patterns help clarify the resonance modes, indicating how magnetic energy is stored and dissipated within the sensor. This understanding is vital for tuning the metamaterial's resonance characteristics to optimize performance.

Fig. 12 illustrates the surface current distribution at the resonant frequencies of 0.437 THz and 0.75 THz, shedding light on the electromagnetic response of the metamaterial. These distributions highlight the pathways of energy flow that underlie the observed resonant behaviour and absorption characteristics. By optimizing the surface current flow, the biosensor's sensitivity can be enhanced, enabling it to detect subtle changes in the biological environment, which is crucial for accurate and reliable diagnostics.

At 0.437 THz, Fig. 12(a) reveals parallel and antiparallel surface current patterns, indicating a strong magnetic response. The antiparallel currents form a circular pattern, suggesting robust magnetic flux in response to the incident H-field. Fig. 12(b) presents the current distribution for the second resonance mode at 0.75 THz, where the direction of current flow, whether parallel or antiparallel, directly influences the distribution of electric and magnetic fields. Parallel currents generate an internal magnetic field that opposes the external H-field, while antiparallel currents enhance the magnetic response. This analysis clarifies the physical absorption processes in the proposed metamaterial structure, providing insights critical for optimizing biosensor design.

Fig. 13 illustrates the power flow distribution within the metamaterial structure at the resonant frequencies of 0.437 THz and 0.75 THz. This analysis highlights the pathways of energy propagation and identifies regions where energy is concentrated and dissipated. Optimizing power flow is essential for improving the biosensor's sensitivity and efficiency in detecting subtle changes in biological samples. At the resonance frequency of 0.437 THz, Fig. 13(a) shows a uniform distribution of power flow, while Fig. 13(b) reveals a dense zone of energy concentration at 0.75 THz. These patterns indicate that the proposed sensor effectively absorbs incident electromagnetic waves.

The electromagnetic characteristics of the proposed dual-band micro-biosensor, designed to function as a metamaterial absorber in the 0–1 THz frequency range, are illustrated in
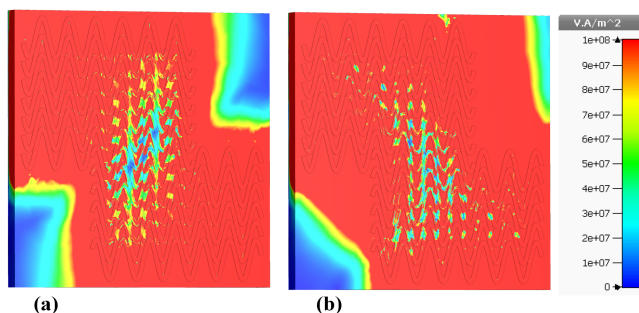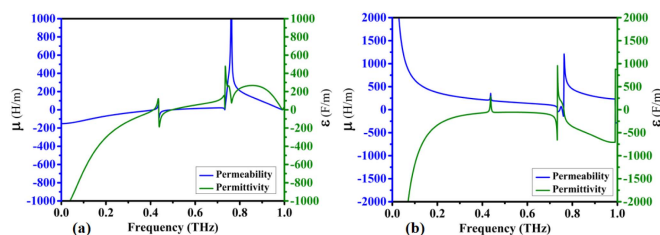

Fig. 14.   Real and imaginary components of permeability (μ) and permittivity (ε) of the proposed metamaterial absorber: (a) real components of μ and ε, and (b) imaginary components of μ and ε.

Figs. 14 to 16. Fig. 14 presents the real and imaginary components of the permeability (μ) and permittivity (ε) of the metamaterial. These graphs depict the material's response to electromagnetic waves across frequencies up to 1 THz.

Fig. 14(a) presents the real parts of permittivity (ε') and permeability (μ'), which correspond to the material's ability to store electric and magnetic energy, respectively. The dual-band nature of the sensor is evident from the distinct resonant peaks within this frequency range, signifying the specific frequencies where the absorber operates most effectively. These resonant peaks highlight the sensor's ability to interact strongly with electromagnetic waves at these frequencies, leading to enhanced sensitivity in detecting changes in the dielectric properties of biological tissues. Consequently, the sensor's accuracy in monitoring or diagnosing biological conditions is significantly improved, as it can respond to subtle variations in tissue properties over these dual bands.

Fig. 14(b) displays the imaginary components of permittivity (ε'') and permeability (μ''), which represent the material's loss factors and are crucial for understanding energy dissipation within the metamaterial. The minimal loss observed at the resonant frequencies ensures high efficiency and sensitivity, making the absorber well-suited for non-invasive diagnostic applications. The behaviour of these imaginary components confirms the material's effectiveness as a perfect absorber in the terahertz range.

Fig. 15(a) shows the impedance characteristics, which are essential for evaluating the absorber's performance. The dual-band nature of the absorber is evident in the two frequency bands where the impedance aligns with that of free space, indicating
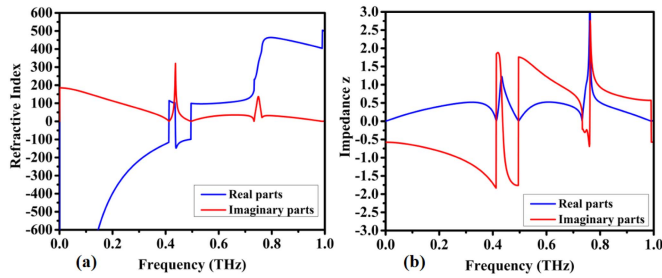
Fig. 15. The proposed metamaterial absorber characterizing responses: (a) real and imaginary parts of the refractive index, and (b) impedance (Z).
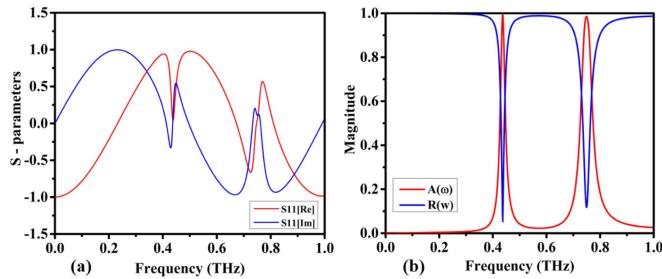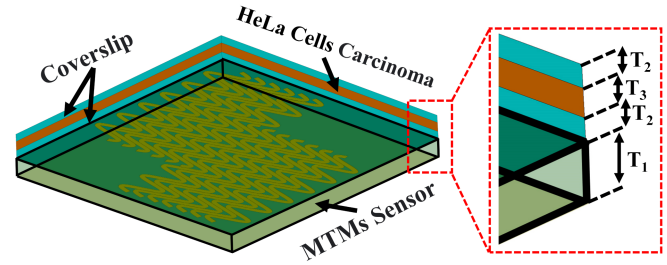

Fig. 17. A layer of biological tissue (either healthy cervical tissue or cancerous cervical tissue) is placed on top of the proposed metamaterial biosensor.

Fig. 16. The proposed metamaterial absorber's: (a) the real & imaginary parts of S_{11}, and (b) reflection (R) & absorption (A) spectra.

optimal absorption. At these resonant frequencies, the sensor is highly effective at detecting changes in the electromagnetic properties of biological tissues, ensuring high sensitivity for biosensing applications.

Fig. 15(b) presents both the real and imaginary parts of the refractive index. The real part indicates how much the wave slows down within the material, while the imaginary part represents the absorption loss. Significant variations in the real part of the refractive index at the resonant frequencies underscore the sensor's dual-band capability. These variations are crucial for fine-tuning the sensor's sensitivity and ensuring accurate detection of dielectric property changes in biological tissues. Additionally, the low absorption loss in the imaginary part at these frequencies further enhances the sensor's efficiency and reliability.

Fig. 16 shows the reflection coefficient (S_{11}), reflection, and absorption spectra of the absorber. Fig. 16(a) shows the real and imaginary parts of S_{11}, which indicate the reflection behaviour of the sensor. The dual-band characteristic is evident from the dips in the magnitude of S_{11} at two specific frequencies, where minimal reflection signifies strong resonance and efficient absorption. These resonant frequencies fall within the target terahertz range, which is crucial for the biosensor's sensitivity and accuracy.

The reflection and absorption spectra shown in Fig. 16(b) highlight two peaks in the absorption spectrum that correspond to the dual-band frequencies. These peaks represent the frequencies at which the metamaterial structure absorbs the maximum amount of incident electromagnetic energy, thereby enhancing the sensor's ability to detect changes in the dielectric constant of

biological tissues. The low reflection values at these frequencies confirm the high efficiency of the absorber.

The relationship between the figures is clear, as the dual-band resonant frequencies are consistently identified across different parameters. The permeability and permittivity analysis in Fig. 14 provides the foundational material properties that influence the impedance, refractive index, and S_{11} parameter responses shown in Figs. 15 and 16. The coherence in the identified resonant frequencies across these figures validates the effectiveness of the design. These comprehensive analyses offer valuable insights for optimizing the micro-biosensor's design and functionality, ensuring effective operation within the desired terahertz frequency bands for early-stage cancer detection.

IV. DIAGNOSIS OF CERVICAL CANCER

The development of a biosensor for cervical cancer diagnostics is crucial for early cancer detection. The proposed metamaterial sensor is designed to identify cervical cancer by analysing its absorption spectra, providing a novel and effective approach for enhancing early detection and prevention.

Research [16], [17], [18], [19], [20] has shown that healthy cervical tissue has a refractive index of 1.368, while malignant tissue has a slightly higher refractive index of 1.392. As illustrated in Fig. 17, the sensor can be used to detect cancerous biological tissue by placing the tissue sample between glass slides and positioning it over the metamaterial sensor. The 0–1 THz frequency range is particularly advantageous for biosensing due to its low water absorption, which allows for deeper tissue penetration. This range also provides distinct spectral fingerprints for biomolecules, facilitating the identification of specific cancer-related markers. Additionally, terahertz radiation is non-ionizing, making it safe for biological applications.

Fig. 18(a) presents the sensor's findings for healthy and cancerous cervical tissue across the 0–1 THz frequency range, with a focus on the initial peak in the 0.41 THz to 0.43 THz region. Fig. 18(b) highlights a significant difference in resonance frequency—specifically 1010 MHz—between healthy and cancerous cervical tissue.

Fig. 19(a) presents the detection results for both cervical cancer and normal cervical tissue, highlighting a second peak in the 0.7 to 0.75 THz range. Fig. 19(b) demonstrates a significant frequency difference of 1690 MHz between cervical cancer and healthy cervical tissue. This notable frequency distinction makes
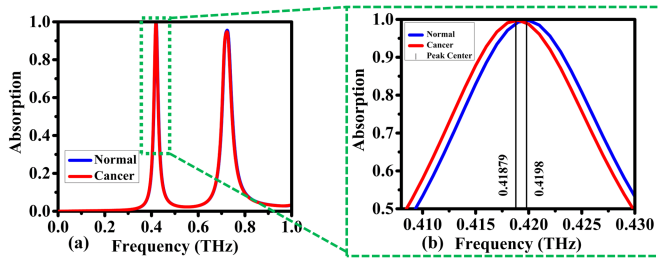
Fig. 18. Absorption coefficient of the proposed biosensor for detecting normal cervical and cervical cancer, (a) 0 - 1 THz, and (b) 0.41 – 0.43 THz.
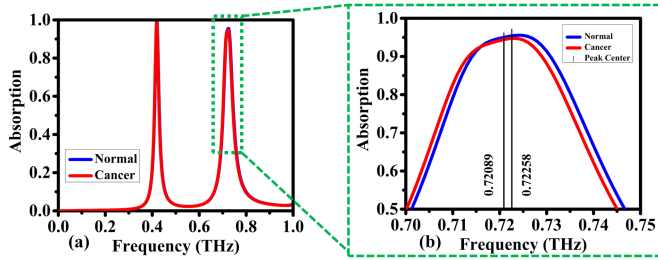

Fig. 19. Absorption coefficient of the proposed biosensor for detecting normal cervical and cervical cancer, (a) 0 - 1 THz, and (b) 0.7 – 0.75 THz.

it feasible to identify cervical cancer using terahertz imaging methods.

A careful examination of the terahertz frequency spectrum of a patient's HeLa cells carcinoma, as shown in Fig. 19, allows medical professionals to accurately diagnose the presence of cervical cancer. This capability facilitates early intervention and treatment, underscoring the potential of the proposed metamaterial sensor in advancing cervical cancer diagnostics.

When evaluating a sensor's performance, sensitivity (S) is a critical parameter that describes its ability to detect small changes in the measured quantity. Sensitivity is generally categorized into two main types: frequency sensitivity and intensity sensitivity. Frequency sensitivity is defined as [5]:

$$S = \frac{\Delta f}{\Delta n} \qquad (3)$$

Where Δf represents the frequency shift of the resonance peak, and Δn denotes the change in the refractive index (RI), typically measured in refractive index units (RIU). This type of sensitivity is crucial for detecting minute variations in the biological environment, which are indicative of pathological changes. Intensity sensitivity, on the other hand, is given by:

$$S = \frac{\Delta I}{\Delta n} \qquad (4)$$

Where ΔI indicates the change in resonant intensity. This measure is particularly important for applications that require precise quantification of analyte concentration based on intensity changes.

The figure of merit (FOM) is another crucial attribute that quantifies a sensor's selectivity. It is defined as the ratio of sensitivity (S) to the full width at half maximum (FWHM) of

the resonant dip, as expressed in [5]:

$$FOM = \frac{S}{FWHM} \qquad (5)$$

A higher figure of merit (FOM) indicates a more selective sensor, capable of distinguishing between small differences in the measured quantity. The quality factor (Q-factor) measures the sharpness of the resonance, which is crucial for achieving high sensitivity. It is determined by the ratio of the resonant wavelength (λ) to the full width at half maximum (FWHM):

$$Q_{factor} = \frac{\lambda}{FWHM} \qquad (6)$$

In terahertz (THz) sensing, metamaterial-based biosensors leverage high Q-factors and sensitivity metrics to achieve enhanced detection capabilities. The unique electromagnetic properties of metamaterials contribute to significant improvements in both sensitivity and figure of merit (FOM), making them highly effective for applications such as early cancer detection and other biomedical diagnostics. By optimizing sensitivity, FOM, and Q-factor, THz metamaterial-based biosensors can deliver superior performance, enabling precise and early detection of biological changes. This underscores their potential as powerful tools in medical diagnostics and various sensing applications [21], [22].

Table II presents a comparative analysis of the proposed metamaterial biosensor alongside previously reported systems in the literature. All these systems utilize the phase change of terahertz waves to obtain data on material properties. Specifically, these sensors exploit changes in the refractive index to

TABLE II
COMPARISON BETWEEN OTHER METAMATERIAL-BASED SENSORS AND THE PROPOSED BIOSENSOR

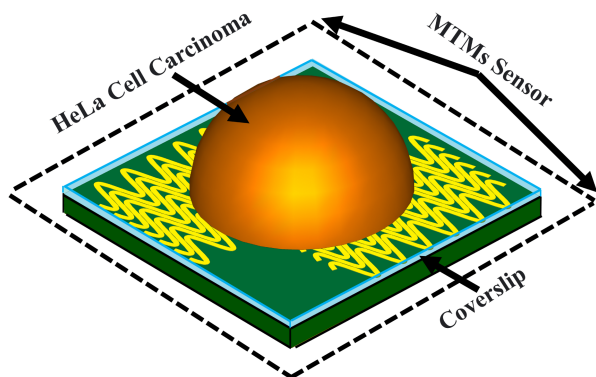| Ref.	Techniques used	Frequency operating (THz)	Material substrate	Absorptivity	Application
[23]	Au/ Dielectric Teflon/Au	1−2.2	dielectric Teflon	0.99	Sensor
[24]	Graphene/ Topas/Au	0.5−4.5	Topas spacer	0.99, 0.98, 0.99	Ultra-Broadband Absorber
[25]	Gold/Silicon Dioxide/ Gold	1.5-1.7	silicon dioxide	0.972, 0.991	Biosensor for Detecting Corona Virus
[26]	Bulk Dirac Semimetal/ Photonic Crystal/Au	1−3	photonic crystal plate	0.97, 0.98, 0.99	Narrowband Perfect Absorber
[27]	Graphene/ Au/ SiO₂/Au	2−6	SiO2	0.99	Refractive Index Sensor
[28]	Au/SiO₂/ Graphene	7-9.5	SiO₂	0.98	Multi-Frequency Broadband and Ultra-Broadband Polarization-Sensitive
[29]	Ion Gel/ Graphene/ Teflon/Gold	0.7-5	Teflon	>0.96	
[30]	PET/FSS/UV glue/ Graphene	0-3	PET	0.99, 0.80, 0.95	Multifunctional Tunable Terahertz
[31]	Au/dielectric layer/Au	1−3	dielectric layer	0.99, 0.99	Sensor
[32]	Glass/InSb/ MgF2/InSb	0-0.37	Glass	0.998	Colon Cancer Detection
[33]	SiO₂/ Graphene	0.5-2.5	SiO₂	-	Breast Cancer Detection
This work	Al/PET/Al	0−1	PET	0.9977, 0.984	Biosensor, Cervical Cancer Diagnostics and Microwave Imaging

Fig. 20. The diagnosis of cervical cancer using the MWI approach.

Fig. 22. The E-field distribution of biological tissue sample at 0.75 THz: (a) healthy cervical, and (b) cervical cancer.

Fig. 21. The E-field distribution of biological tissue sample at 0.437 THz: (a) healthy cervical, and (b) cervical cancer.
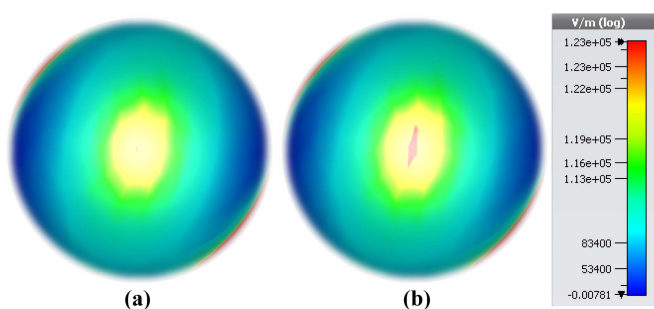

Fig. 23. The H-field distribution of biological tissue sample at 0.437 THz: (a) healthy cervical, and (b) cervical cancer.

affect absorption spectra, a principle that this study applies to differentiate between healthy and cancerous tissue.

The urgent need for early identification and effective treatment of cervical cancer highlights the importance of accurately distinguishing malignant tissue. In terms of performance, particularly absorptivity, the proposed biosensor compares favourably with benchmark devices. Additionally, it features a compact physical size, which is crucial for practical applications, such as needing smaller biopsy samples for diagnostics.

Fig. 20 illustrates the application of the proposed biosensor, showing the testing of a cervical sample placed on a coverslip. Fig. 21(a) depicts a normal cervical scan, which reveals a weak electric field. In contrast, Fig. 21(b) shows an area of red, indicating a very high electric field density, characteristic of cancerous tissue. Further distinction is provided by examining the electric field at the second peak of 0.75 THz, as shown in Fig. 22. Fig. 22(a) presents a region with a very low electric field, corresponding to a healthy cervix, while Fig. 22(b) shows a region with high electric field density, indicative of cervical cancer.

To validate these electric field findings, a parallel examination of the magnetic field is conducted, as demonstrated in Fig. 23. The results from detecting the H-field are consistent with the electric field observations, reinforcing the reliability and effectiveness of the proposed metamaterial biosensor in distinguishing between healthy and cancerous cervical tissue.
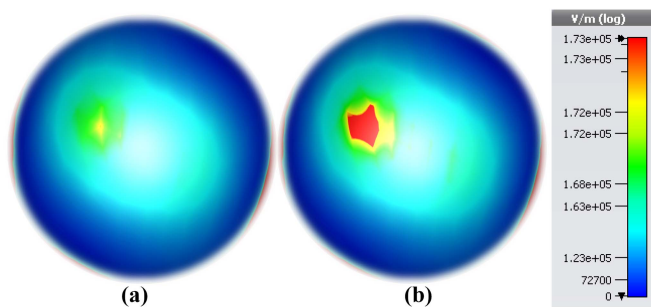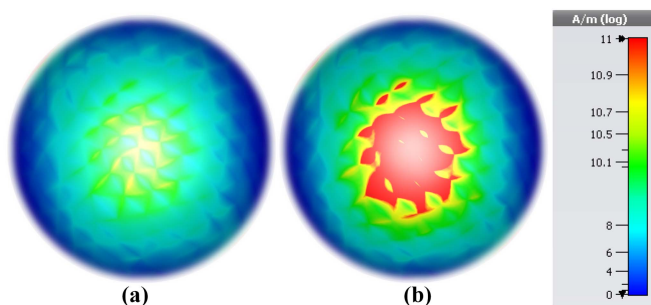
V. FUTURE PERSPECTIVE

These results demonstrate that early-stage diagnosis of various cancers, including breast cancer, colon cancer, adrenal gland cancer (such as PC-12 tumors), and non-melanoma skin cancer, can be significantly enhanced using terahertz electromagnetic wave imaging biosensors. These advanced biosensors utilize THz EM waves to detect subtle changes in tissue properties that are indicative of cancerous growth.

Terahertz imaging is particularly advantageous for early cancer detection due to its ability to penetrate biological tissues with minimal damage and its sensitivity to variations in tissue composition and structure. By analyzing the interaction of THz waves with different types of tissues, these biosensors can identify specific signatures associated with early-stage tumors, improving diagnostic accuracy and enabling timely intervention.

For breast cancer, THz imaging can reveal abnormal tissue changes before they become visible through traditional imaging techniques. Similarly, for colon cancer, THz biosensors can detect precancerous lesions and early-stage tumors by differentiating between healthy and malignant tissue based on their unique THz absorption and reflection characteristics.

In the case of adrenal gland cancer (PC-12), THz imaging can be used to distinguish between benign and malignant lesions, facilitating early diagnosis and appropriate treatment planning. Non-melanoma skin cancer detection benefits from THz imaging's ability to differentiate between cancerous and healthy skin tissues with high precision.

TABLE III
COMPARISON OF THE PROPOSED BIOSENSOR'S PERFORMANCE METRICS WITH OTHER METAMATERIAL-BASED BIOSENSORS

Ref.	Year Published	FOM (RIU^{-1})	Q	S (THz/RIU)	Bio-application
[34]	2017	-	-	0.0242, 0.02438	Detection of Virus
[35]	2021	-	-	0.074	Cervical cancer
[36]	2022	-	-	0.068	Hepatocellular Carcinoma Sensor
[37]	2022	1.81, 1.57	8.21, 6.05	0. 203	
[38]	2023	-	11	0.278	Bovin Serum Albumin Protein
[39]	2023	0.86, 1.15	12.8, 13.5	0.0515, 0.076	Non-Melanoma Skin Cancer Diagnostics
This work	-	1.9589, 1.529	20.382, 16.286	0.042, 0.0704	Cervical Cancer Diagnostics

FOM: Figure of merit, RIU-I: Refractive index unit

Overall, the use of THz electromagnetic wave imaging biosensors offers a promising approach for early cancer detection across various types of cancers, enhancing diagnostic capabilities and potentially improving patient outcomes through earlier intervention and more accurate monitoring.

VI. BENCHMARKING

The proposed terahertz dual-band metamaterial biosensor represents a significant advancement over traditional microwave imaging techniques for cervical cancer diagnostics. This biosensor, designed as a metamaterial perfect absorber, operates within the 0-1 THz range and exhibits dual-band functionality. It achieves impressive absorption rates of 99.77% and 98.4% at its first and second resonant peaks, respectively (see Table II).

Table III compares the performance metrics of the proposed biosensor with other metamaterial-based biosensors, showing that it has a sensitivity of 0.042 THz/RIU at the first peak and 0.0704 THz/RIU at the second peak, with quality factors (Q-factors) of 20.382 and 16.286, respectively. The figures of merit (FOM) for the proposed biosensor are 1.9589 RIU^{-1} and 1.529 RIU^{-1} at these peaks, indicating its high precision and efficiency.

Unlike conventional sensors, the compact size of this metamaterial biosensor allows for the use of significantly smaller biopsy samples, facilitating less invasive testing procedures. Its high sensitivity and specificity are crucial for early-stage cancer detection, ensuring accurate identification of abnormalities in biological tissues. The superior performance metrics of this biosensor, coupled with its practical advantages, highlight its potential as a highly effective tool for non-invasive cervical cancer diagnostics.

VII. CONCLUSION

This research highlights the potential of utilizing metamaterial structures as biosensors for the early detection of cancerous biological tissues. The underlying mechanism is based on the ability of cancerous cells to alter the effective dielectric constant of the surrounding tissue. This alteration leads to a shift in the resonance frequency of the metamaterial sensor, enabling the detection of cancerous changes at an early stage.

One of the key advantages of the proposed metamaterial biosensor is its compact size. Unlike traditional sensors, which often require larger sample sizes, this sensor's dimensions are independent of the wavelength, allowing it to analyze significantly smaller biopsy samples. This compact nature not only reduces the invasiveness of the procedure but also improves patient comfort.

Furthermore, the biosensor has demonstrated effectiveness in identifying abnormalities within biological tissues, providing a valuable tool for early cancer detection. The ability to detect subtle changes in tissue properties makes it particularly useful for monitoring and diagnosing various forms of cancer at a stage when treatment options are most effective.

Overall, this research underscores the promising capabilities of metamaterial-based biosensors in enhancing diagnostic accuracy and facilitating earlier intervention in cancer treatment. The compact design and high sensitivity of the biosensor contribute to its potential as a powerful tool for advancing medical diagnostics.

USE OF HUMAN PARTICIPANTS

There were no humans involved in the study.

COMPETING INTERESTS

The authors declare no competing interests.

DATA AVAILABILITY

The datasets used and/or analyzed during the current study are available from the first author on reasonable request.

AUTHOR CONTRIBUTIONS

Conceptualization: M.N.H. (Musa N. Hamza), M.A. (Mohammad Alibakhshikenari), B.V. (Bal Virdee), M.H (Muhamad A. Hamad) & S.Kh. (Salahuddin Khan); Data curation: M.N.H. & S.K. (Slawomir Koziel); Formal analysis: M.N.H. & B.V.; Visualization: M.N.H., M.A, S.Kh. and S.K.; Writing—original draft: M.N.H., M.A, B.V., M.H. and S.K.; Writing—review and editing: M.A, B.V., S.Kh., S.K, and E.L.; Software: M.N.H.; Resources: M.N.H., M.A, M.H. and S.K.; Supervision: M.A, B.V. and S.K.

REFERENCES

[1] H. Sung et al., "Global cancer statistics 2020: GLOBOCAN estimates of incidence and mortality worldwide for 36 cancers in 185 countries," *CA: Cancer J. Clinicians*, vol. 71, no. 3, pp. 209–249, May 2021.
[2] H. Udagawa et al., "Liposomal eribulin for advanced adenoid cystic carcinoma, gastric cancer, esophageal cancer, and small cell lung cancer," *Cancer Med.*, vol. 12, no. 2, pp. 1269–1278, Jan. 2023.
[3] F. Bray, J. Ferlay, I. Soerjomataram, R. L. Siegel, L. A. Torre, and A. Jemal, "Global cancer statistics 2018: GLOBOCAN estimates of incidence and mortality worldwide for 36 cancers in 185 countries," *CA: Cancer J. Clinicians*, vol. 68, no. 6, pp. 394–424, Nov. 2018.
[4] P. U. Jepsen, D. G. Cooke, and M. Koch, "Terahertz spectroscopy and imaging – Modern techniques and applications," *Laser Photon. Rev.*, vol. 5, no. 1, pp. 124–166, 2011.
[5] A. H. Aly, A. A. Ameen, M. A. Mahmoud, Z. S. Matar, M. Al-Dossari, and H. A. Elsayed, "Photonic crystal enhanced by metamaterial for measuring electric permittivity in GHz range," *Photonics*, vol. 8, no. 10, 2021, Art. no. 416.

[6] A. Siemion, L. Minkevičius, L. Qi, and G. Valušis, "Spatial filtering based terahertz imaging of low absorbing objects," *Opt. Lasers Eng.*, vol. 139, Apr. 2021, Art. no. 106476.

[7] H. Liu, S. Zhang, and J. Han, "Microwave sensing using metamaterial absorbers," *Appl. Phys. Lett.*, vol. 99, no. 17, 2011, Art. no. 174101.

[8] N. I. Landy, S. Sajuyigbe, J. J. Mock, D. R. Smith, and W. J. Padilla, "Perfect metamaterial absorber," *Phys. Rev. Lett.*, vol. 100, no. 20, 2008, Art. no. 207402.

[9] I. A. Al-Naib, C. Jansen, and M. Koch, "High-Q terahertz resonances in all-dielectric metamaterials," *Appl. Phys. Lett.*, vol. 103, no. 10, 2013, Art. no. 101101.

[10] B. Liu et al., "Terahertz ultrasensitive biosensor based on wide-area and intense light-matter interaction supported by QBIC," *Chem. Eng. J.*, vol. 462, 2023, Art. no. 142347.

[11] Y. Peng et al., "Three-step one-way model in terahertz biomedical detection," *PhotoniX*, vol. 2, pp. 1–18, 2021.

[12] M. Askari, H. Pakarzadeh, and F. Shokrgozar, "High Q-factor terahertz metamaterial for superior refractive index sensing," *J. Opt. Soc. Amer. B*, vol. 38, no. 12, pp. 3929–3936, 2021.

[13] O. Ramadan, "Stability-improved ADE-FDTD implementation of drude dispersive models," *IEEE Antennas Wireless Propag. Lett.*, vol. 17, no. 5, pp. 877–880, May 2018.

[14] S. Li et al., "A polarization-independent fiber-optic SPR sensor," *Sensors*, vol. 18, no. 10, 2018, Art. no. 3204.

[15] M. Abdelsalam, A. M. Mahmoud, and M. A. Swillam, "Polarization independent dielectric metasurface for infrared beam steering applications," *Sci. Rep.*, vol. 9, no. 1, 2019, Art. no. 10824.

[16] K. Ahmed, B. K. Paul, F. Ahmed, M. A. Jabin, and M. S. Uddin, "Numerical demonstration of triangular shaped photonic crystal fibre-based biosensor in the Terahertz range," *IET Optoelectron.*, vol. 15, no. 1, pp. 1–7, 2021.

[17] M. A. Jabin et al., "Surface plasmon resonance based titanium coated biosensor for cancer cell detection," *IEEE Photon. J.*, vol. 11, no. 4, Aug. 2019, Art. no. 3700110.

[18] P. Kumar, V. Kumar, and J. S. Roy, "Dodecagonal photonic crystal fibers with negative dispersion and low confinement loss," *Optik*, vol. 144, pp. 363–369, 2017.

[19] T. Parvin, K. Ahmed, A. M. Alatwi, and A. N. Z. Rashed, "Differential optical absorption spectroscopy-based refractive index sensor for cancer cell detection," *Opt. Rev.*, vol. 28, pp. 134–143, 2021.

[20] P. Sharma, P. Sharan, and P. Deshmukh, "A photonic crystal sensor for analysis and detection of cancer cells," in *2015 Int. Conf. Pervasive Comput.*, 2015, pp. 1–5.

[21] M. Gómez-Castaño, J. L. Garcia-Pomar, L. A. Pérez, S. Shanmugathasan, S. Ravaine, and A. Mihi, "Electrodeposited negative index metamaterials with visible and near infrared response," *Adv. Opt. Mater.*, vol. 8, no. 19, 2020, Art. no. 2000865.

[22] R. Krause et al., "Ultrafast charge separation in bilayer WS2/graphene heterostructure revealed by time-and angle-resolved photoemission spectroscopy," *Front. Phys.*, vol. 9, 2021, Art. no. 668149.

[23] A. S. Saadeldin, M. F. O. Hameed, E. M. A. Elkaramany, and S. S. A. Obayya, "Highly sensitive terahertz metamaterial sensor," *IEEE Sensors J.*, vol. 19, no. 18, pp. 7993–7999, Sep. 2019.

[24] L. Liu, W. Liu, and Z. Song, "Ultra-broadband terahertz absorber based on a multilayer graphene metamaterial," *J. Appl. Phys.*, vol. 128, no. 9, 2020, Art. no. 093104.

[25] Z. El-Wasif, T. Ismail, and O. Hamdy, "Design and optimization of highly sensitive multi-band terahertz metamaterial biosensor for coronaviruses detection," *Opt. Quantum Electron.*, vol. 55, no. 7, 2023, Art. no. 604.

[26] Y. Wang et al., "Terahertz tunable three band narrowband perfect absorber based on dirac semimetal," *Physica E: Low-Dimensional Syst. Nanostructures*, vol. 131, 2021, Art. no. 114750.

[27] M.-R. Nickpay, M. Danaie, and A. Shahzadi, "Highly sensitive THz refractive index sensor based on folded split-ring metamaterial graphene resonators," *Plasmonics*, vol. 17, pp. 237–248, 2022.

[28] Z. Chen et al., "Graphene multi-frequency broadband and ultra-broadband terahertz absorber based on surface plasmon resonance," *Electronics*, vol. 12, no. 12, 2023, Art. no. 2655.

[29] S. Asgari and T. Fabritius, "Numerical simulation and equivalent circuit model of multi-band terahertz absorber composed of double-sided graphene comb resonator array," *IEEE Access*, vol. 11, pp. 36052–36063, 2023.

[30] S. Zhuang et al., "Graphene-based absorption–transmission multi-functional tunable THz metamaterials," *Micromachines*, vol. 13, no. 8, 2022, Art. no. 1239.

[31] B.-X. Wang, Y. He, P. Lou, and W. Xing, "Design of a dual-band terahertz metamaterial absorber using two identical square patches for sensing application," *Nanoscale Adv.*, vol. 2, no. 2, pp. 763–769, 2020.

[32] Z. Vafapour, W. Troy, and A. Rashidi, "Colon cancer detection by designing and analytical evaluation of a water-based THz metamaterial perfect absorber," *IEEE Sensors J.*, vol. 21, no. 17, pp. 19307–19313, Sep. 2021.

[33] C. Tan et al., "Cancer diagnosis using terahertz-graphene-metasurface-based biosensor with dual-resonance response," *Nanomaterials*, vol. 12, no. 21, 2022, Art. no. 3889.

[34] S. Park, S. Cha, G. Shin, and Y. Ahn, "Sensing viruses using terahertz nano-gap metamaterials," *Biomed. Opt. Exp.*, vol. 8, no. 8, pp. 3551–3558, 2017.

[35] D. Li et al., "Identification of early-stage cervical cancer tissue using metamaterial terahertz biosensor with two resonant absorption frequencies," *IEEE J. Sel. Topics Quantum Electron.*, vol. 27, no. 4, Jul./Aug. 2021, Art. no. 8600107.

[36] R. Bhati and A. K. Malik, "Ultra-efficient terahertz metamaterial sensor," *Results Opt.*, vol. 8, 2022, Art. no. 100236.

[37] H. Hu, B. Qi, Y. Zhao, X. Zhang, Y. Wang, and X. Huang, "A graphene-based THz metasurface sensor with air-spaced structure," *Front. Phys.*, vol. 10, 2022, Art. no. 990126.

[38] Y. Shen et al., "Low-concentration biological sample detection using an asymmetric split resonator terahertz metamaterial," *Photonics*, vol. 10, no. 2, 2023, Art. no. 111.

[39] M. N. Hamza and M. T. Islam, "Designing an extremely tiny dual-band biosensor based on MTMs in the terahertz region as a perfect absorber for non-melanoma skin cancer diagnostics," *IEEE Access*, vol. 11, pp. 136770–136781, 2023.